2746 *Chem. Mater.* **2009,** *21,* 2746–2754
DOI:10.1021/cm9003917

CHEMISTRY OF MATERIALS
Article

Ion Irradiation of Ternary Pyrochlore Oxides

Gregory R. Lumpkin,* Katherine L. Smith, Mark G. Blackford, and Karl R. Whittle

Institute of Materials Engineering, Australian Nuclear Science and Technology Organisation, Private Mail Bag 1, Lucas Heights, New South Wales 2234, Australia

Elizabeth J. Harvey and Simon A. T. Redfern

Department of Earth Sciences, University of Cambridge, Downing Street, Cambridge, CB2 3EQ

Nestor J. Zaluzec

Materials Science Division, Argonne National Laboratory, 9700 South Cass Avenue, Argonne, Illinois 60439

Received February 10, 2009. Revised Manuscript Received April 29, 2009

Polycrystalline synthetic samples of $Y_2Ti_{2-x}Sn_xO_7$ with $x = 0.4$, 0.8, 1.2, and 1.6, together with $Nd_2Zr_2O_7$, $Nd_2Zr_{1.2}Ti_{0.8}O_7$, and $La_{1.6}Y_{0.4}Hf_2O_7$, were irradiated in situ in the intermediate voltage electron microscope (IVEM)-Tandem Facility at Argonne National Laboratory using 1.0 MeV Kr ions at temperatures of 50 to 650 K. Determination of the critical amorphization fluence (F_c) as a function of temperature has revealed a dramatic increase in radiation tolerance with increasing Sn content on the pyrochlore B site. Nonlinear least-squares analysis of the fluence-temperature curves gave critical temperatures (T_c) of 666 ± 4, 335 ± 12, and 251 ± 51 K for the $Y_2Ti_{2-x}Sn_xO_7$ samples with $x = 0.4$, 0.8, and 1.2, respectively. The sample with $x = 1.6$ appears to disorder to a defect fluorite structure at a fluence below 1.25×10^{15} ions cm^{-2} and remains crystalline to 5×10^{15} ions cm^{-2} at 50 K. Additionally, the critical fluence-temperature response curves were determined for $Nd_2Zr_{1.2}Ti_{0.8}O_7$ and $La_{1.6}Y_{0.4}Hf_2O_7$, and we obtained T_c values of 685 ± 53 K and 473 ± 52 K, respectively, for these pyrochlores. $Nd_2Zr_2O_7$ did not become amorphous after a fluence of 2.5×10^{15} ions cm^{-2} at 50 K, but there is evidence that it may amorphize at a higher fluence, with an estimated T_c of ~135 K. The observed T_c results are discussed with respect to the predicted T_c values based upon a previously published empirical model (Lumpkin, G. R.; Pruneda, M.; Rios, S.; Smith, K. L.; Trachenko, K.; Whittle, K. R.; Zaluzec, N. J. *J. Solid State Chem.* **2007**, *180*, 1512). In the $Y_2Ti_{2-x}Sn_xO_7$ pyrochlores, T_c appears to be linear with respect to composition, and is linear with respect to r_A/r_B and $x(48f)$ for all samples investigated herein.

1. Introduction

Oxide minerals of the pyrochlore group $A_{2-m}B_2X_{6-w}$-$Y_{1-n}\cdot pH_2O$ are well-known in nature as potential ores of Nb and Ta and as hosts of Th, U, lanthanides, and other high-field-strength elements in highly evolved magmatic and hydrothermal systems.[1−4] The ideal pyrochlore structure type has also been of considerable interest over the years because of a range of potentially useful properties such as fast-ion (mainly anion) conductivity, electrical conductivity, and geometrically frustrated magnetism.[5−10] The compositions of these oxide pyrochlores are extremely diverse, with numerous III−IV and II−V compounds, among others, conforming to the ideal stoichiometry, $A_2B_2X_6Y$. Furthermore, many synthetic defect pyrochlores (e.g., $A_2B_2X_6$, AB_2X_6, and B_2X_6M, where M is a cation located on the normally anionic Y-site)[11] have been synthesized and evaluated for their metal-insulating behavior and ionic (mainly proton and small cation) conductivity.[12]

Pyrochlore is also one of the principal actinide host phases in titanate ceramics designed for the safe disposal

*Corresponding author. Phone: +61 (0) 2 9717 3742. Fax: +61 (0) 2 9543 7179. E-mail: grl@ansto.gov.au.

(1) Williams, C. T.; Wall, F.; Woolley, A. R.; Phillipo, S. *J. Afr. Earth Sci.* **1997**, *25*, 137.
(2) Lumpkin, G. R.; Chakoumakos, B. C.; Ewing, R. C. *Am. Mineral.* **1986**, *71*, 569.
(3) Lumpkin, G. R.; Ewing, R. C. *Am. Mineral.* **1996**, *81*, 1237.
(4) Wall, F.; Williams, C. T.; Woolley, A. R.; Nasraoui, M. *Mineral. Mag.* **1996**, *60*, 731.
(5) Heremans, C.; Wuensch, B. J.; Stalick, J. K.; Prince, E. *J. Solid State Chem.* **1995**, *117*, 108–121.
(6) Raju, N. P.; Dion, M.; Gingras, M. J. P.; Mason, T. E.; Greedan, J. E. *Phys. Rev. B* **1999**, *59*, 14489–14498.
(7) Lee, J. S.; Moon, S. J.; Noh, T. W.; Takeda, T.; Kanno, R.; Yoshii, S.; Sato, M. *Phys. Rev. B* **2005**, *72*, 035124.
(8) Groult, D.; Pannetier, J.; Raveau, B. *J. Solid State Chem.* **1982**, *41*, 277.
(9) Ehlert, M. K. G., J.E.; Subramanian, M. A. *J. Solid State Chem.* **1988**, *75*, 188–196.
(10) Whittle, K. R.; Lumpkin, G. R.; Ashbrook, S. E. *J.Solid State Chem.* **2006**, *179*, 512–521.
(11) Chakoumakos, B. C. *J. Solid State Chem.* **1984**, *53*, 120–129.
(12) Subramanian, M. A.; Aravamudan, G.; Rao, G. V. S. *Prog. Solid State Chem.* **1983**, *15*, 55–143.

 Published on Web 05/26/2009

of actinide-rich nuclear wastes, including weapons Pu.[13−17] Radiation damage effects in pyrochlores have been studied extensively using ion irradiation techniques that cater specifically to the determination of damage models and mechanisms on short time scales and under strictly controlled conditions as a function of ion mass, energy, and flux onto the specimen.[18] Such ion irradiation studies, in particular those conducted on thin TEM specimens, have elucidated the effects of composition and structure on the critical amorphization fluence (F_c), and the critical temperature (T_c) above which the material remains crystalline. Results of these studies document the critical temperature for amorphization as the pyrochlore structure becomes more fluoritelike.[19−23] Recent atomistic computer simulations, employing empirical interatomic potential models to calculate "static" defect energies, suggest that both cation antisite and anion Frenkel defect energies play an important role in determining the radiation "tolerance" of III−IV pyrochlore compounds.[24,25]

In this work, we examine the variation in radiation response of several ternary pyrochlore oxides using in situ ion irradiation methods. One particular approach to understanding the factors that control radiation tolerance is the development of empirical models to predict T_c based upon a set of material properties as independent variables. In previous work, we developed simple models for the estimation of T_c using existing ion irradiation data (e.g., 1.0 MeV Kr) for simple binary oxide pyrochlore compounds.[23] These models are based on linear combinations of independent variables, including crystal structure parameters, ionic radius ratios, electronegativity data, and published defect formation energies obtained from atomistic computer simulations. When compared with contour maps of the defect energies,[25] a contour map of predicted T_c versus the radii of the A-site and B-site cations,[23] indicates that defect energies should be highly correlated with T_c for B-site cations with radii greater than about 0.067 nm.

As there appears to be no a priori reason to believe that pyrochlore compounds within a solid solution series will behave linearly in radiation response, we conducted ion irradiation studies of compositions across the $Y_2Ti_{2-x}Sn_xO_7$ pyrochlore series (denoted YTS). These samples are of interest because the existing data for the Ti and Sn end-members reveal a large difference (~800 K) in the critical temperature (T_c), even though there is little, if any, difference in the degree of intrinsic disorder.[26] In addition to the YTS samples, we have included samples of $Nd_2Zr_2O_7$ and $Nd_2Zr_{1.2}Ti_{0.8}O_7$ (denoted NTZ) as they provide an independent test of the radiation response due to substitution on the B-site of the pyrochlore structure. Finally, we also compare the behavior of $La_2Hf_2O_7$ and $La_{1.6}Y_{0.4}Hf_2O_7$ pyrochlores (denoted LYH) in order to examine the effect of substitution on the A-site.

2. Experimental Procedures

(A) Synthesis and Characterization. Experimental procedures are summarized only briefly here, as extensive details have been published elsewhere.[27−30] Polycrystalline ceramic samples were prepared by conventional mixed metal oxide methods using stoichiometric amounts of La_2O_3, Nd_2O_3, Y_2O_3, SnO_2, TiO_2, ZrO_2, and HfO_2 (generally 99.5−99.9% purity). Starting materials were ground together in stoichiometric proportions, pressed into pellets, and heated at 1773 K in air for 48 h. The samples were reground and heated again in air at the same temperature for up to 96 h. The YTS samples were examined using a Bruker D8 X-ray diffractometer with monochromatic Cu $K\alpha_1$ radiation (1.5406 Å) and a tuned Sol-X detector. Neutron diffraction experiments were conducted on NTZ samples using the high flux time-of-flight diffractometer POLARIS at the ISIS pulsed spallation neutron facility, Rutherford Appleton Laboratory, U.K.. The two LYH samples used in this study are from our work in progress on the system $La_{2-x}Y_xHf_2O_7$; these have been studied by neutron diffraction using the C2 spectrometer at Chalk River, Canada; the results of these diffraction studies are described in detail elsewhere.[27] All diffraction patterns were analyzed using the Rietveld method, to determine the structure that agrees best the recorded data. For the YTS samples, we estimated the $x(48f)$ coordinate to an accuracy of about ±0.005 by finding the best fit to the observed versus calculated X-ray diffraction peak intensities (minimum R-factor method). Microstructural features of the samples were determined by scanning electron microscopy (SEM) of polished sections using JEOL JSM-6400 and JSM-820 instruments. Semiquantitative microanalyses of the YTS and LYH samples were obtained using a Noran Voyager energy dispersive spectrometer (EDX) attached to the JSM-6400, while quantitative analyses of the NTZ samples were performed using a Cameca SX100 electron probe microanalysis (EPMA) system. Additional details of the experimental procedures are given in recent publications and will not be repeated here.[28,29]

(13) Ball, C. J.; Buykx, W. J.; Dickson, F. J.; Hawkins, K. D.; Levins, D. M.; Smart, R. S. C.; Smith, K. L.; Stevens, G. T.; Watson, K. G.; Weedon, D.; White, T. J. *J. Am. Ceram. Soc.* **1989**, *72*, 404–414.
(14) Ewing, R. C.; Weber, W. J.; Clinard, F. W. *Prog. Nucl. Energy* **1995**, *29*, 63–127.
(15) Lumpkin, G. R. *J. Nucl. Mater.* **2001**, *289*, 136–166.
(16) Lumpkin, G. R.; Smith, K. L.; Gieré, R.; Williams, C. T. In Energy, Waste and the Environment: A Geochemical Perspective; Gieré, R., Stille, P., Eds.; Geological Society: London, 2004; Vol. 236, pp 89−111.
(17) Lumpkin, G. R. *Elements* **2006**, *2*, 365–372.
(18) Ewing, R. C.; Lian, J.; Wang, L. M. In Radiation Effects and Ion Beam Modification of Materials; Wang, L. M., Fromknecht, R., Snead, L. L., Downey, D. F., Takahashi, H., Eds.; Materials Research Society: Boston, 2004; Vol. 792, pp 37−48.
(19) Lian, J.; Chen, J.; Wang, L. M.; Ewing, R. C.; Farmer, J. M.; Boatner, L. A.; Helean, K. B. *Phys. Rev. B* **2003**, *68*, 134107.
(20) Lian, J.; Ewing, R. C.; Wang, L. M.; Helean, K. B. *J. Mater. Res.* **2004**, *19*, 1575–1580.
(21) Lumpkin, G. R.; Whittle, K. R.; Rios, S.; Smith, K. L.; Zaluzec, N. J. *J. Phys.: Condens. Matter* **2004**, *16*, 8557–8570.
(22) Lian, J.; Helean, K. B.; Kennedy, B. J.; Wang, L. M.; Navrotsky, A.; Ewing, R. C. *J. Phys. Chem. B* **2006**, *110*, 2343.
(23) Lumpkin, G. R.; Pruneda, J. M.; Rios, S.; Smith, K. L.; Trachenko, K.; Whittle, K. R.; Zaluzec, N. J. *J. Solid State Chem.* **2007**, *180*, 1512–1518.
(24) Minervini, L.; Grimes, R. W.; Sickafus, K. E. *J. Am. Ceram. Soc.* **2000**, *83*, 1873–1878.
(25) Sickafus, K. E.; Minervini, L.; Grimes, R. W.; Valdez, J. A.; Ishimaru, M.; Li, F.; McClellan, K. J.; Hartmann, T. *Science* **2000**, *289*, 748–751.
(26) Wuensch, B. J.; Eberman, K. W.; Heremans, C.; Ku, E. M.; Onnerud, P.; Yeo, E. M. E.; Haile, S. M.; Stalick, J. K.; Jorgensen, J. D. *Solid State Ionics* **2000**, *129*, 111–133.
(27) Whittle, K. R.; Cranswick, L. M.; Redfern, S. A. T.; Swainson, I. P.; Lumpkin, G. R. *J. Solid State Chem.* **2009**, *182*, 442–450.
(28) Ashbrook, S. E.; Whittle, K. R.; Lumpkin, G. R.; Farnan, I. *J. Phys. Chem. B* **2006**, *110*, 10358–10364.
(29) Harvey, E. J.; Whittle, K. R.; Lumpkin, G. R.; Smith, R. I.; Redfern, S. A. T. *J. Solid State Chem.* **2005**, *178*, 800–810.
(30) Lumpkin, G. R.; Whittle, K. R.; Rios, S.; Smith, K. L.; Zaluzec, N. J. *J. Solid. State Chem.* **2004**, *16*(47), 8557–8570.

(B) Ion Irradiation Experiments. TEM samples were prepared by crushing small ceramic fragments in methanol and collecting the suspension on holey carbon-coated copper grids. Samples were characterized prior to the irradiation experiments using a JEOL 2000FXII TEM operated at 200 kV and calibrated for selected area diffraction over a range of objective lens currents using a gold film standard. The compositions of the grains were checked by thin film EDX analysis procedures using a Link ISIS energy dispersive spectrometer attached to the TEM.[31] Ion irradiation experiments with 1.0 MeV Kr ions were carried out in situ at the IVEM-Tandem User Facility at Argonne National Laboratory using a Hitachi TEM interfaced to a NEC ion accelerator.[32] All TEM observations were carried out using an accelerating potential of 300 kV. Ion irradiations were performed at temperatures of 50−650 K with the electron beam of the TEM turned off, using a counting rate of 100 counts s^{-1} and a flux of 6.25×10^{11} ions cm^{-2} s^{-1} within a beam of ~2 mm diameter. Each sample was irradiated using incremental irradiation steps and selected grains were observed using bright field imaging and selected area electron diffraction after each irradiation step. The critical amorphization fluence (F_c) was determined from the last fluence increment in which weak Bragg diffraction spots were observed and the next increment for which only diffuse rings occur in the diffraction pattern. For each sample, we determined F_c from the average of several grains. For a more detailed description of the irradiation procedures, readers should consult recently published work.[33]

3. Results

(A) Structure and Composition. All of the YTS samples appear to be single phase[27−29] and exhibit the classical powder diffraction pattern characteristics of the ordered pyrochlore structure.[28] The lattice parameter increases linearly with increasing Sn content ($a = 0.0135x + 1.01$, $R^2 = 0.9966$). Using the minimum R-factor method noted above, we found x(48*f*) values of 0.322−0.339 for the six samples with increasing Sn content. These are in reasonable agreement with values of x(48*f*) from published neutron data, [26] but they do show a wider range, and thus we have chosen to use estimates of x(48*f*) based on more accurate neutron diffraction results shown in Figure 5a of Wuensch et al.[26] We note that Wuensch et al.[26] also refined the occupancies of the 48*f*, 8*a*, and 8*b* sites in their YTS samples and found no significant evidence for the intrinsic oxygen disorder often observed in other systems. In previous work on these samples using ^{89}Y nuclear magnetic resonance (NMR) spectroscopy, Ashbrook et al. [28] suggested that the A-site is fully occupied by Y and the B-site is randomly occupied by Ti and Sn across the solid-solution series.

SEM-EDX results[28] also indicate that the YTS samples are essentially single phase and close to the nominal starting compositions. Minor variations in composition were observed for the samples with $x = 0.4$, 0.8, and 1.2. Considering the analytical fitting errors of approximately ±0.05 atoms per formula unit, together with additional smaller errors of ±0.01−0.02 atoms per formula unit due to counting statistics, the YTS samples are reasonably close to the ideal $A_2B_2O_7$ stoichiometry of pyrochlore (e.g., within ±2 standard deviations). TEM-EDX results confirmed the compositions and general quality of the samples at image magnifications similar to those to be used in the in situ irradiation experiments. Selected area electron diffraction patterns of all YTS samples are consistent with the ordered pyrochlore structure, e.g., they exhibit strong superstructure diffracted beams such as those with 111, 311, 331, 333/511, and 531 Miller indices.[28]

The two NTZ samples used in this study, $Nd_2Zr_2O_7$ and $Nd_2Zr_{1.2}Ti_{0.8}O_7$, were previously examined by neutron diffraction and electron probe microanalysis by Harvey et al.[29] Both samples are essentially single phase and the SEM-EDX and EPMA data indicate that they are close to their nominal compositions. Although the anion site occupancies were not refined, both samples appear to be well-ordered on the basis of the occurrence of relatively intense pyrochlore superlattice peaks in the neutron powder diffraction patterns.[29] This was confirmed by electron diffraction. Samples with higher Ti contents in the NTZ system consist of pyrochlore and a monoclinic, layered $Nd_2Ti_2O_7$ perovskite phase (the two-phase region exists between ~55 and 5 mol % $Nd_2Zr_2O_7$).

Neutron powder diffraction patterns[27] demonstrate that the two LYH samples, $La_2Hf_2O_7$ and $La_{1.6}Y_{0.4}Hf_2O_7$, also exhibit relatively intense pyrochlore superlattice peaks, consistent with the electron diffraction observations on crystals in [110] zone axis orientations. Refinement of the 48*f*, 8*a*, and 8*b* anion site occupancy parameters revealed that both samples are fully ordered. However, our work on other samples in the LYH system indicates that intrinsic anion disorder begins in the sample with Y = 0.8 atoms per formula unit and thereafter, the disorder increases in the pyrochlore phase with increasing Y content. Furthermore, this system consists of coexisting pyrochlore and defect fluorite phases for Y = 1.6 atoms per formula unit. Hence, a greater range of compositions in the LYH series has not been explored in this study. Microanalyses obtained by SEM-EDX and TEM-EDX methods confirm that the two samples used in this study are single-phase and reasonably close to their nominal compositions.

(B) Monte Carlo Simulations. To assess the effect of sample thickness and composition on defect production, stopping power, and energy transfer to the atoms of the solid, we have performed Monte Carlo simulations for the YTS, NTZ, and LYH pyrochlores using the binary collision approximation (BCA) as implemented in SRIM-2006.[34] For these calculations, we have produced the full damage cascades, averaged over 1000 ions, assuming displacement energies of 50 eV and binding energies of 3 eV for all atoms. Calculated densities were used on the basis of the measured lattice parameter and nominal composition

(31) Lumpkin, G. R.; Smith, K. L.; Blackford, M. G.; Gieré, R.; Williams, C. T. *Micron* **1994**, *25*, 581–587.
(32) Allen, C. W.; Funk, L. L.; Ryan, E. A. In Ion-Solid Interactions for Materials Modification and Processing; Poker, D. B., Ila, D., Cheng, Y. T., Harriott, L. R., Sigmon, T. W., Eds.; Materials Research Society: Warrendale, PA, 1996; Vol. 396, pp 641−646.
(33) Lumpkin, G. R.; Smith, K. L.; Blackford, M. G.; Thomas, B. S.; Whittle, K. R.; Marks, N. A.; Zaluzec, N. J. *Phys. Rev. B* **2008**, *77*, 212401.
(34) Ziegler, J. F. *Nucl. Instrum. Methods Phys. Res., Sect. B* **2004**, *219−20*, 1027–1036.

Table 1. Results of Monte Carlo Simulations of Damage Production, Linear Energy Transfer (LET) and Electronic/Nuclear Stopping Powers, $(dE/dx)_e$ and $(dE/dx)_n$, for $Y_2Ti_{2-x}Sn_xO_7$, $La_2Hf_2O_7$, $La_{1.6}Y_{0.4}Hf_2O_7$, $Nd_2Zr_2O_7$, and $Nd_2Ti_{1.2}Zr_{0.8}O_7$ Pyrochlores[a]

sample	LET (eV ion^{-1} nm^{-1})	$(dE/dx)_e$ (eV nm^{-1})	$(dE/dx)_n$ (eV nm^{-1})	ENSP ratio
$Y_2Ti_2O_7$	1540	960	1294	0.744
$Y_2Ti_{1.6}Sn_{0.4}O_7$	1580	958	1312	0.733
$Y_2Ti_{1.2}Sn_{0.8}O_7$	1620	960	1333	0.722
$Y_2Ti_{0.8}Sn_{1.2}O_7$	1700	1141	1556	0.731
$Y_2Ti_{0.4}Sn_{1.6}O_7$	1740	1139	1574	0.726
$Y_2Sn_2O_7$	1830	1141	1597	0.713
$La_2Hf_2O_7$	1610	945	1375	0.688
$La_{1.6}Y_{0.4}Hf_2O_7$	1650	935	1383	0.681
$Nd_2Zr_2O_7$	1530	897	1308	0.687
$Nd_2Ti_{0.8}Zr_{1.2}O_7$	1590	916	1314	0.702

[a] ENSP is the ratio of electronic to nuclear stopping power.

of each sample. Results of the simulations are listed in Table 1. For typical TEM specimen thicknesses of 50−100 nm, the mean linear energy transfer (LET) of the YTS samples ranges from 1540 to 1830 eV ion^{-1} nm^{-1} and the ratio of the electronic to nuclear stopping power (ENSP) ranges from 0.75 to 0.71. SRIM simulations show that the NTZ samples have LET values of 1590−1530 eV ion^{-1} nm^{-1} and ENSP values of 0.70−0.69 with increasing Zr content. Similarly, the LYH samples have LET values of 1610−1650 eV ion^{-1} nm^{-1} and ENSP values of 0.69−0.68 with increasing Y content.

Over the same thickness interval of 50−100 nm, the linear damage production increases from about 7−9 damage events ion^{-1} nm^{-1} for $Y_2Ti_2O_7$ to 10−12 damage events ion^{-1} nm^{-1} for $Y_2Sn_2O_7$. Values for the LYH and NTZ samples fall within this range. The resulting number of atomic displacements (N_d) is shown as a function of thickness for the two end-members of the YTS pyrochlore series in Figure 1. The narrow envelope illustrated here encompasses the calculated displacements for all samples investigated in this study. For specimen thicknesses of 50−100 nm, Figure 1 indicates that the average number of displacements per ion varies from about 290−330 to 680−770.

(C) Ion Irradiation Damage. We did not irradiate $Y_2Ti_2O_7$ in this study as the radiation response of this material was reported in previous experiments.[35] Representative electron diffraction patterns shown in Figure 2 illustrate the typical progression of damage observed in the YTS pyrochlore series for samples with $x = 0.4$ and $x = 0.8$. Because the temperature response differs between the two samples, we have given the fluence for each SAED pattern in terms of the fraction of the critical fluence (F_c) listed in Table 2. For the sample with $x = 0.4$, close to the [110] zone axis, diffuse scattering from amorphous domains becomes apparent around 0.4 F_c, together with a decrease in the intensity of many of the Bragg beams indicative of the pyrochlore superlattice. This situation is typical of materials that become amorphous

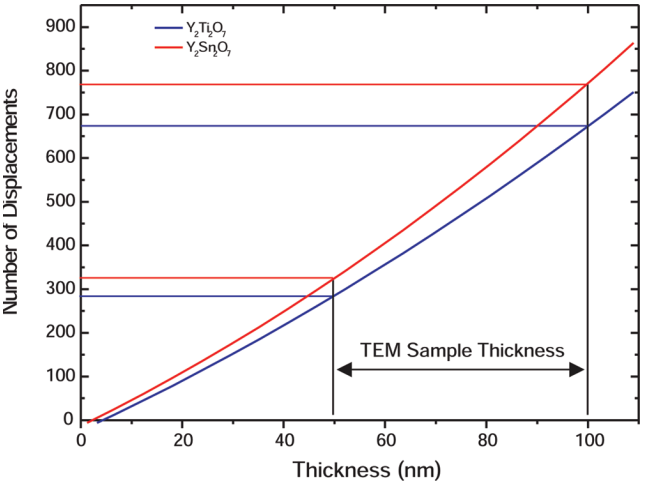

Figure 1. Plot showing the predicted number of displacements against thickness for $Y_2Ti_2O_7$ and $Y_2Sn_2O_7$. The predictions were made using SRIM-2006 with displacement energies of 50 eV and the measured densities for the samples.

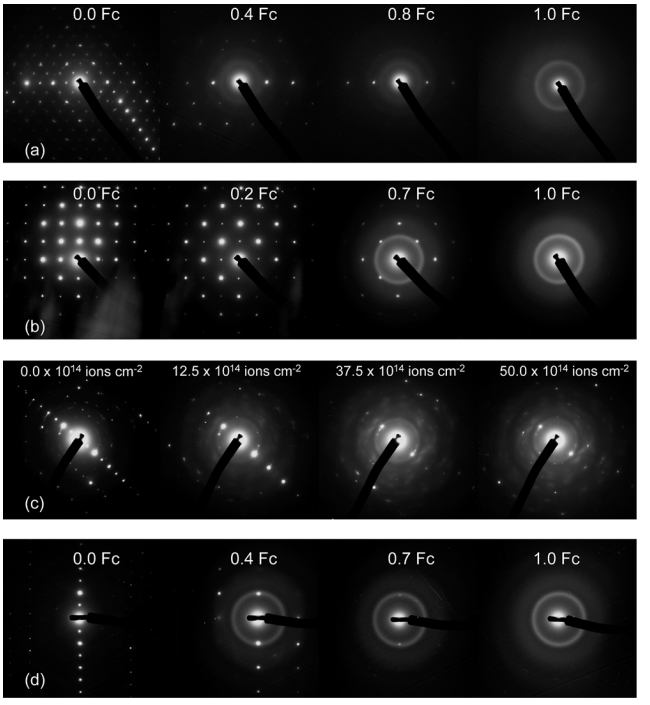

Figure 2. Selected area diffraction patterns for (a) $Y_2Sn_{0.4}Ti_{1.6}O_7$, (b) $Y_2Sn_{0.8}Ti_{1.2}O_7$, (c) $Y_2Sn_{1.2}Ti_{0.8}O_7$, and (d) $Nd_2Zr_{1.2}Ti_{0.8}O_7$. The partial values of fluence (F_c) are relative to the critical fluence for amorphization for (a), (b), and (d). The fluences in ions cm^{-2} for (c) are quoted, as this system did not go amorphous.

and is indicative of the coexistence of amorphous and crystalline regions in the material. At a damage level of 0.8 F_c, most of the Bragg beams have disappeared in this compound. The fully amorphous material is characterized by diffuse scattering into two broad rings with real space peak positions of approximately 0.18 and 0.30 nm. This diffuse scattering is similar to that observed in many other synthetic and natural pyrochlore compounds and is related to the pair correlation functions of the atoms in the aperiodic structure.[36]

(35) Wang, S. X.; Wang, L. M.; Ewing, R. C.; Kutty, K. V. G. *Nucl. Instrum. Methods Phys.Res., Sect. B* **2000**, *169*, 135–140.

(36) Lumpkin, G. R.; Ewing, R. C. *Phys. Chem. Miner.* **1988**, *16*, 2–20.

Table 2. Average Critical Amorphization Fluence Values (and errors) for YTS Pyrochlores with $x = 0.4$, 0.8, and 1.2 Following Irradiation with 1.0 MeV Kr ions[a]

$x = 0.4$		$x = 0.8$		$x = 1.2$	
T (K)	F_c	T (K)	F_c	T (K)	F_c
50	5.6 (0.4)	50	5.6 (0.4)	50	11.7 (1.1)
302	6.4 (0.6)	150	6.7 (0.3)	100	9.8 (0.8)
400	7.5 (1.8)	250	9.4 (0.9)	175	17.2 (1.6)
450	6.5 (0.7)	302	23.4 (3.1)	200	20.8 (5.0)
600	12.8 (1.8)				
650	46.9 (3.1)				

[a] All fluence values are given in units of 10^{14} ions cm^{-2}. Errors represent one standard deviation on the mean of several measurements at each temperature. We also irradiated the sample with $x = 1.6$, but it remained crystalline up to a fluence of 50×10^{14} ions cm^{-2} at 50 K.

The YTS sample with $x = 0.8$ is oriented near the [100] zone axis and exhibits a loss of intensity in alternate diffracted beams at 0.2 F_c; however, the diffuse scattering associated with discrete amorphous domains is not easily seen at this fluence. Diffuse scattering does appear at some fluence between 0.2 and 0.7 F_c and the scattering in the fully amorphous sample is nearly identical to that observed in the sample with $x = 0.4$. At the relative fluence value of 0.7 F_c, the weaker alternate diffracted beams are no longer observed and only a few of the strong Bragg beams remain. Similar results were obtained for the YTS sample with $x = 1.2$ (not shown in Figure 2). The sample with $x = 1.6$ showed damage in the form of a very weak ring in the selected area electron diffraction pattern but did not become amorphous upon irradiation up to a fluence of 5×10^{15} ions cm^{-2} at 50 K (see Figure 2). The weak ring in this sample is not a broad as normally observed in these and other oxides upon amorphization. Thus, there appears to be a significant difference in the details of damage between this sample and those with $x = 0.0-1.2$. Furthermore, at $x = 1.6$, the Bragg beams indicative of the pyrochlore superlattice disappear quickly with increasing fluence and the crystals show evidence of localized diffuse scattering. We did not irradiate $Y_2Sn_2O_7$, as this compound was previously shown[22] to remain crystalline up to a fluence of 47.5×10^{15} ions cm^{-2} at 25 K.

We also found that the $La_{1.6}Y_{0.4}Hf_2O_7$ and $Nd_2Zr_{1.2}Ti_{0.8}O_7$ samples are susceptible to amorphization by irradiation with 1.0 MeV Kr ions and the progression of damage revealed by electron diffraction is similar to that described above for the YTS pyrochlores for $x < 1.6$. Experimental results are given in Table 3. Representative SAED patterns of $Nd_2Zr_{1.2}Ti_{0.8}O_7$ near the (111) reciprocal lattice row are shown in the bottom row of Figure 2. With increasing ion fluence, a diffuse ring is readily observed at 0.4 F_c and the diffuse scattering in the fully amorphous sample is nearly identical to that found in the other amorphous pyrochlores. There is a corresponding decrease in intensity of the Bragg beams up to 0.7 F_c, with the weaker alternate beams disappearing at 0.4 F_c, in a sequence that is generally observed in all of the samples that become amorphous. The binary oxide pyrochlore $Nd_2Zr_2O_7$ did not become amorphous upon irradiation to a fluence of 25×10^{14} ions cm^{-2} at 50 K, but it did show evidence of damage in the form of a diffuse ring in the SAED pattern. Thus it is possible that this compound will amorphize at a much higher fluence.

Table 3. Average Critical Amorphization Fluence Values (and errors) for $La_{1.6}Y_{0.4}Hf_2O_7$, $Nd_2Zr_{1.2}Ti_{0.8}O_7$, and the Zirconolite Standard Following Irradiation with 1.0 MeV Kr ions[a]

$La_{1.6}Y_{0.4}Hf_2O_7$		$Nd_2Zr_{1.2}Ti_{0.8}O_7$		zirconolite std	
T (K)	F_c	T (K)	F_c	T (K)	F_c
50	7.5 (0.7)	50	3.9 (0.5)	302	3.8 (0.2)
150	8.8 (1.8)	303	5.3 (0.6)		
250	18.8 (3.8)	500	15.6 (3.0)		
298	26.6 (3.1)	550	18.0 (1.6)		
350	38.5 (3.6)				

[a] All fluence values are given in units of 10^{14} ions cm^{-2}. Errors represent one standard deviation on the mean of several measurements at each temperature. We also investigated $Nd_2Zr_2O_7$ and this sample remained crystalline up to a fluence of 25×10^{14} ions cm^{-2} at 50 K.

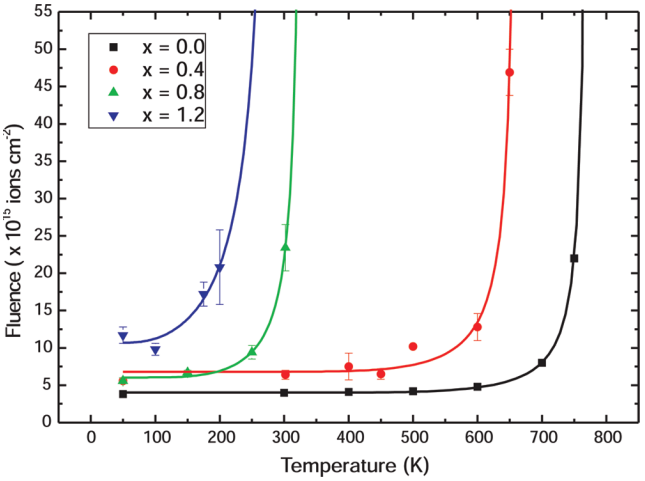

Figure 3. Critical fluence against temperature for $Y_2Ti_2O_7$, $Y_2Ti_{1.6}Sn_{0.4}O_7$, $Y_2Ti_{1.2}Sn_{0.8}O_7$, and $Y_2Ti_{0.8}Sn_{1.2}O_7$. The data are fitted using eq 1; the numerical results for $Y_2Ti_{1.6}Sn_{0.4}O_7$, $Y_2Ti_{1.2}Sn_{0.8}O_7$, and $Y_2Ti_{0.8}Sn_{1.2}O_7$ are shown in Table 4. The values for $Y_2Ti_2O_7$ are from Lian et al.[19]

The ion irradiation results of this study are shown graphically in Figures 3 and 4, including data for $Y_2Ti_2O_7$ taken from the previous work of Wang et al.[35] The critical fluence versus temperature data are fitted to eq 1 below[37]

$$F_c = \frac{F_{c0}}{1 - \exp\left[\left(\frac{E_a}{k_b}\right)\left(\frac{1}{T_c} - \frac{1}{T}\right)\right]} \qquad (1)$$

In this equation, F_c is the critical amorphization fluence, F_{c0} is the critical fluence at 0 K, E_a is the activation energy for recovery of radiation damage, k_b is the Boltzmann constant, T_c is the critical temperature above which the specimen remains crystalline, and T is the temperature of the experiment. The critical fluence extrapolated to 0 K, critical temperature, and activation energy for recovery of damage were determined by nonlinear least-squares refinement of the data listed in Tables 2 and 3, weighted according to $1/\sigma^2$, where σ is the reported error on the critical fluence. Allowing all three parameters to vary, the

(37) Weber, W. J. *Nucl. Instrum. Methods Phys. Res., Sect. B* **2000**, *166–167*, 98–106.

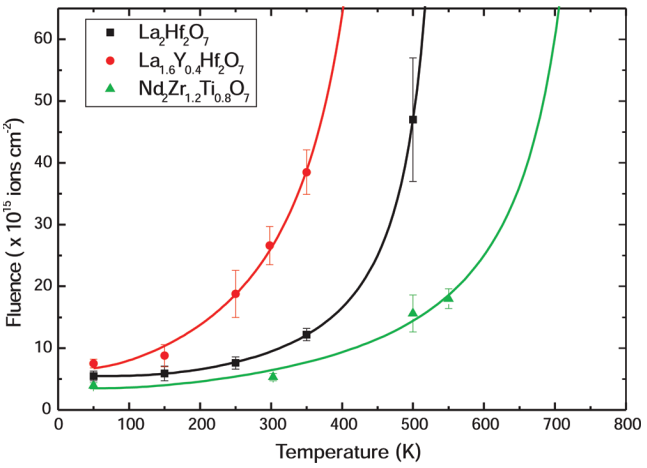

Figure 4. Critical fluence against temperature for $La_2Hf_2O_7$, $La_{1.6}Y_{0.4}Hf_2O_7$, and $Nd_2Zr_{1.2}Ti_{0.8}O_7$. The data are fitted using eq 1 and are shown in Table 3.

Table 4. Numerical Results (and errors) Obtained from the Fitting of Fluence-Temperature Data Using eq 1 for $Y_2Ti_{2-x}Sn_xO_7$ pyrochlores with x = 0.4, 0.8, and 1.2; $La_{1.6}Y_{0.4}Hf_2O_7$; and $Nd_2Zr_{1.2}Ti_{0.8}O_7$[a]

sample	F_{c0}	T_c (K)	T_c (K) calcd[b]	E_a (eV)[c]	E_a (eV)[d]
$Y_2Ti_2O_7$	4.0	780	895	0.4	1.18−1.58
$Y_2Ti_{1.6}Sn_{0.4}O_7$	5.9 (0.3)	666 (4)	718	0.31 (0.08)	1.10−1.36
$Y_2Ti_{1.2}Sn_{0.8}O_7$	6.2 (0.3)	335 (12)	548	0.08 (0.02)	0.55−0.69
$Y_2Ti_{0.8}Sn_{1.2}O_7$	10.4 (0.8)	251 (51)	373	0.05 (0.03)	0.42−0.52
$La_2Hf_2O_7$	5.5 (0.7)	563 (22)	527	0.05 (0.01)	0.92−1.15
$La_{1.6}Y_{0.4}Hf_2O_7$	7.3 (0.7)	473 (52)	466	0.02 (0.01)	0.78−0.97
$Nd_2Ti_{0.8}Zr_{1.2}O_7$	3.8 (0.5)	685 (53)	588	0.06 (0.02)	1.11−1.39

[a] All fluence values are given in units of 1014 ions cm−2. [b] Obtained using eq 2 in Lumpkin et al.[23] The error on T_c associated with this equation is 81 K. Calculated T_c values were also obtained for YTS pyrochlores with x = 1.6 (194 K), x = 2.0 (21 K), and for $Nd_2Zr_2O_7$ (238 K). [c] Obtained from eq 1 in this paper. [d] Obtained from eq 2 in this paper.

numerical results of these refinements are reported in Table 4. We have observed that F_{c0} is generally negatively correlated with r_A/r_B and positively correlated with $x(48f)$; however, there are insufficient data at high F_{c0} to determine the functional form of these relationships.

As expected, the observed T_c decreases with increasing Sn, Zr, and Y content in the YTS, NTZ, and LYH samples, respectively. In the YTS system, T_c effectively decreases from 780 to ~0 K on substitution of 80% Sn for Ti on the B-site. Similarly, our results for the NTZ samples indicate that the substitution of 40% Zr for Ti on the B-site induces a very large change in the radiation response, wherein T_c decreases from 685 K to a miminum value of 50 K based on the observation of a weak diffuse ring in the $Nd_2Zr_2O_7$ sample at the maximum quoted fluence in this experiment. For the LYH samples, the results indicate that the substitution of 20% Y for La on the A-site leads to a decrease in T_c from 563 to 473 K. In Figure 5, we show the observed T_c values as functions of r_A/r_B and $x48f$. Although the data for r_A/r_B may be nonlinear for >800 K, for the present data set a linear function is adequate, resulting in a value of r_A/r_B = 1.496 when extrapolated to 0 K (Figure 5a). This exercise gives the threshold value of r_A/r_B ,below which these ternary pyrochlore oxides are radiation tolerant. A similar exercise was conducted using the $x48f$ data set, giving a threshold value of 0.3354 above which these ternary pyrochlore oxides are radiation tolerant (Figure 5b). Both extrapolations correctly predict that $Y_2Sn_2O_7$ should be radiation tolerant and that $Nd_2Zr_2O_7$ should be subject to amorphization with $T_c \approx 80-190$ K.

The predicted T_c values obtained from eq 2 in Lumpkin et al.[23] are also given in Table 4. For the YTS samples, we plotted the T_c values versus composition in Figure 6a, where we can see that the observed values are systematically lower than the critical temperatures calculated from the empirical model. An extrapolation of the linear fit to the observed data beyond x = 1.2 reaches a temperature of 0 K just above x = 1.6, which is reasonably consistent with the experimental observations. The NTZ samples are somewhat inconsistent in terms of the predicted radiation response, thus we find that the predicted T_c for $Nd_2Zr_{1.2}Ti_{0.8}O_7$ is 97 K lower than the observed value (although the values are within error of one another), whereas the predicted T_c for $Nd_2Zr_2O_7$ is 238 K, which is 103 K higher than the value of 135 K obtained from an average of the two estimates in Figure 5. Considering the experimental errors and the error of ± 81 K associated with eq 2 in Lumpkin et al.,[23] the observed and calculated T_c values of the two LYH samples are in excellent agreement with one another. For comparison, we have also plotted the observed and calculated T_c data for the $Gd_2Ti_{2-x}Zr_xO_7$ system (denoted GTZ) in Figure 6b, where the experimental data are from the work of Wang et al.[38] On the basis of the linear fits, the agreement between the observed and predicted critical temperatures is excellent; however, the individual T_c values for the intermediate GTZ samples with x = 0.5 and 1.0 are underestimated by 201 K and overestimated by 141 K, respectively.

The activation energies returned by the use of eq 1 are quite low for all of the samples, ranging from as little as 0.02 eV for $La_{1.6}Y_{0.4}Hf_2O_7$ to 0.44 eV for $Y_2Ti_2O_7$. To further investigate the activation energies, we have employed an alternative method to estimate E_a using the fitted values of $F_{c,0}$ and T_c together with the known ion flux of the experiment, according to the relationship[37] shown in eq 2

$$T_c = \frac{E_a}{[k_B \ln(F_{c0}\nu/\phi)]} \quad (2)$$

In eq 2, ν is the effective attempt frequency, σ_a is the cross section for amorphization ($\sigma_a = 1/F_{c0}$), and ϕ is the ion flux. This equation can be rearranged to calculate E_a using the data listed in Table 4. Thus we have calculated a range of E_a values for the samples by assuming a range of ν values from 1×10^9 to 1×10^{12} s^{-1}. The results obtained using this procedure suggest that the activation energies range from about 0.4 to 1.6 eV.

4. Discussion

Monte Carlo simulations based on the BCA method indicate that the TEM specimens irradiated in this study should experience similar levels of damage production, e.g.,

(38) Wang, S. X.; Begg, B. D.; Wang, L. M.; Ewing, R. C.; Weber, W. J.; Kutty, K. V. G. *J. Mater. Res.* **1999**, *14*, 4470–4473.

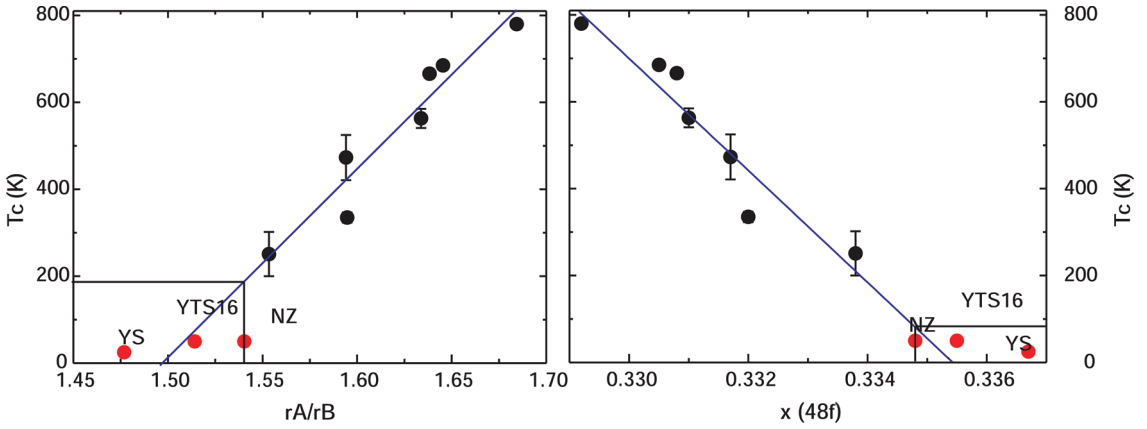

Figure 5. Plots of critical temperature (T_c) against r_A/r_b and $x(48f)$; the labeled spots correspond to those materials that did not go amorphous and their predicted positions.

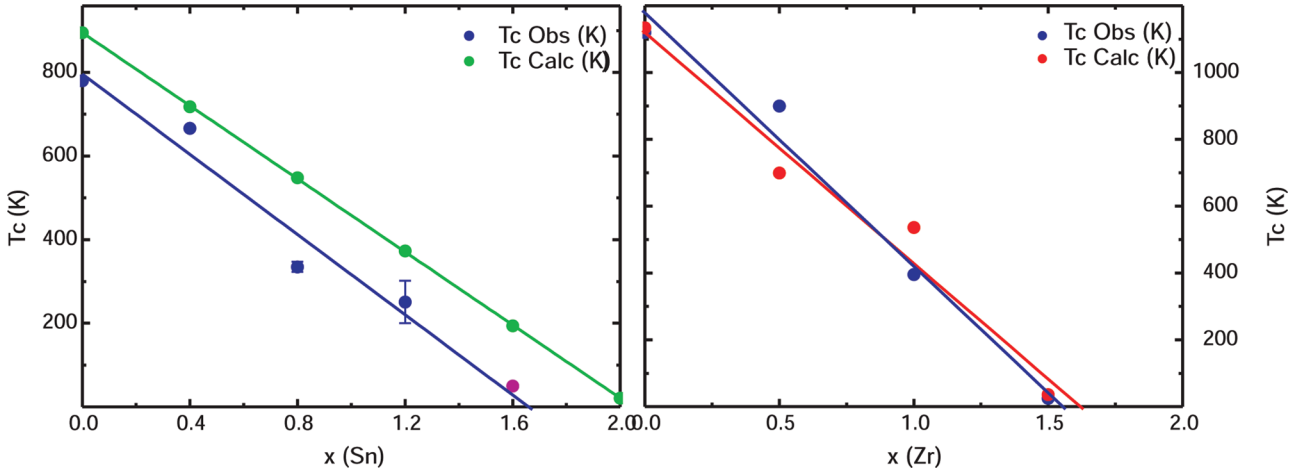

Figure 6. Plots of critical temperature (T_c) against Sn and Zr content in $Y_2Ti_{2-x}Sn_xO_7$ and $Gd_2Ti_{2-x}Zr_xO_7$, showing measured and predicted values.

generally between 7 and 12 damage events ion^{-1} nm^{-1} for typical thicknesses of 50−100 nm. The damage production translates to a global average of approximately 310−725 displacements per ion over the same range of sample thickness. Because of the general lack of experimental determinations for displacement energy of a cation of a crystal site (E_d), we have assumed that E_d = 50 eV for all atoms in this study. On the basis of the results of several recent molecular dynamics (MD) simulations of the threshold displacement energies in pyrochlore compounds in which the E_d values for cations are predicted to be as high as 200 eV or more,[39,40] the number of displaced atoms per ion could be considerably lower than indicated in Figure 1. We have previously illustrated (see Figure 4 in Lumpkin et al.[21]) the effect of increased E_d values on defect production for $La_2Zr_2O_7$, and on the basis of those results, we suggested that it is unlikely that differences in the E_d values provide an explanation for the observed behavior at low temperature. Although some variation in the number of displaced atoms per ion may occur as a function of sample thickness, the LET and ENSP values reported earlier in this paper also suggest that the damage mechanism will be similar for all YTS, NTZ, and LYH samples.

Given the preceding discussion, the main recourse for this work is to understand the large changes in radiation response in these pyrochlores in terms of structure, bonding, and energetics of defect formation and migration. In the YTS system, the large difference in the fluence-temperature response under in situ irradiation in the TEM with 1.0 MeV Kr ions is quite remarkable. On the basis of the the neutron structure refinements of Wuensch and co-workers,[26] it appears that all of the pyrochlores in this system are highly ordered; therefore, the presence of intrinsic disorder does not seem to play a major role in the radiation response. This is confirmed by refinements of the anion site occupancies in the LYH samples, in which we find no evidence for intrinsic disorder. In earlier work, we have shown that T_c for certain III−IV pyrochlore-defect fluorite compounds can be modeled empirically by using the $x(48f)$ oxygen coordinate, lattice parameter (a_0), electronegativity of the B-site cation (X_{pB}), and the combined anion-Frenkel and cation antisite disorder energy (E_{dis}). In this model, the E_{dis} values are estimated from static defect calculations based on empirical potentials covering a wide range of III−IV pyrochlore composition space.[24] According to eq 2 in Lumpkin et al.,[23] radiation tolerance (e.g., lower T_c for amorphization) is correlated with higher $x(48f)$

(39) Chartier, A.; Meis, C.; Crocombette, J. P.; Corrales, L. R.; Weber, W. J. *Phys. Rev. B* **2003**, *67*, 174102.
(40) Devanathan, R.; Weber, W. J. *J. Appl. Phys.* **2005**, *98*, 086110.

values and with lower values of the other parameters. On the basis of the actual changes in the $x(48f)$ oxygen coordinate, a_0, X_{pB}, and E_{dis}, across each solid-solution series, we evaluated the weight of each parameter in determining the change in the calculated T_c value. For the YTS pyrochlores, the parameter weights are −249 for x (48f), 174 for a_0, 240 for X_{pB}, and −1040 for E_{dis}. Therefore, this model indicates that the effect of E_{dis} is about 4−6 times greater than the other independent variables. In this case, the competing effect of the higher X_{pB} of the Sn cation is overcome by the energetics of disorder.

The results discussed above suggest that the radiation tolerance of YTS pyrochlores correlates with the combined disorder formation energies. This is consistent with the observation that the sample with $x = 1.6$ appears to disorder to a defect fluorite structure at a fluence below 1.25×10^{15} ions cm^{-2} and remains crystalline to 5×10^{15} ions cm^{-2} at 50 K. We refrain from suggesting that the other pyrochlores shown in Figure 2 undergo the same order−disorder transformation. Our caution relates to the nature of electron scattering in crystals that become amorphous under irradiation, wherein the material consists of both crystalline and amorphous domains that coexist over a finite dose range. Because of dynamic scattering effects, especially for strongly scattering materials like pyrochlores, one must account for complex scattering interactions between the crystalline regions, amorphous domains, and defects. Under these conditions, as the fraction of crystalline material decreases with increasing fluence, the scattering in crystalline domains changes from a dynamic to a kinematic-like state. Thus, the intensities of dynamically enhanced superlattice reflections may decrease dramatically and disappear to background levels as the volume of the amorphous phase increases. Fortunately, the situation is much simpler for the compounds (e.g., YTS16) that remain crystalline and do not accumulate a significant fraction of amorphous material. In this situation, the changes observed in the SAED patterns are likely to be a correct indication of an order−disorder mechanism. We will address this electron scattering phenomenon in detail elsewhere.

Parameter weights obtained from eq 2 in Lumpkin et al.[23] for the NTZ samples are −143 for $x(48f)$, 101 for a_0, −48 for X_{pB}, and −260 for E_{dis}, indicating that the effect of E_{dis} is 2−5 times greater than the other independent variables. In this system, which has a larger A-site cation and substitution of Zr for Ti on the B-site, the structural parameters appear to play a greater role in the model prediction and the X_{pB} of Zr now induces a small negative effect on T_c. For the LYH pyrochlores, the substitution of Y for La on the A-site reduces r_A/r_B and promotes increased radiation tolerance. Furthermore, in this case, there is no effect of electronegativity as the B-site cation is always Hf, so in this system, we find parameter weights of −23 for $x(48f)$, −38 for a_0, and −173 for E_{dis}, indicating that the effect of E_{dis} is 4−8 times greater than the structural parameters. Overall, this analysis suggests that the combined defect formation energies play a major role in determining the radiation response of pyrochlores in all three systems studied herein.

With regard to the predictive capability of the empirical model discussed above, the observed T_c values of the YTS pyrochlores differ from the predicted values by an average of about −110 K. This systematic difference exceeds the standard deviation of the predictive model and suggests that the data used to derive the model, based on binary oxide pyrochlores, are insufficient to describe the behavior of the YTS samples across this region of III−IV pyrochlore space. Part of the problem relates to the lack of observational data for pyrochlores with B-site cations of intermediate ionic radius between Ti (r_B = 0.0605 nm) and Sn (r_B = 0.069 nm). There is significant scope to study samples with B = Ru (r_B = 0.062 nm) and Mo (r_B = 0.065 nm) as well as other ternary pyrochlore solid-solutions. For the NTZ samples irradiated in this study, the predicted T_c values are somewhat better, with the value for $Nd_2Zr_2O_7$ being overestimated and the value for $Nd_2Zr_{1.2}Ti_{0.8}O_7$ being underestimated (both by ∼100 K). The ternary pyrochlore $Nd_2Zr_{1.2}Ti_{0.8}O_7$ is also in a region of III−IV pyrochlore space that has not been previously explored by ion irradiation. The predicted T_c values for the LYH pyrochlores are in excellent agreement with the observed values, and it is noteworthy that there are a number of experimental observations on binary oxide pyrochores in this part of the A−B cation radius space.

As noted in the introduction, there is no reason to assume that a solid-solution series will behave linearly in T_c, as competing factors may lead to complex behavior as a function composition, structure, and bonding. This has been observed, for example, in the $La_xSr_{1-1.5x}TiO_3$ perovskite system where a minimum in T_c is found at $x = 0.2$ and appears to be related to the inversion of defect interactions.[41,42] Although our data set for the YTS pyrochlore system is limited, the observed critical temperatures shown in Figure 6a appear to follow a linear trend. In general, this is consistent with the individual parameter correlations illustrated in Figure 5 and furthermore, an extrapolation of the linear trend provides a reasonably accurate estimate of the behavior of the YTS16 sample (see Figure 6a). Thus it appears that this solid-solution series is essentially linear in T_c, suggesting that the experimental data for the ternary pyrochlore oxides examined in this study can be used to produce updated empirical models for amorphization of III−IV pyrochlores. Examination of the experimental data for the GTZ system[38] is consistent with the preceding discussion (see Figure 6b).

Although a minor consideration of this study, the accurate assessment of activation energies is an ongoing problem in the study of radiation effects and this is especially true for the case of in situ ion irradiation of thin TEM specimens. A number of investigators have employed eq 1 for analysis of critical fluence versus temperature data obtained using thin crystals and have noted that the E_a values obtained from least-squares fits are unusually low

(41) Smith, K. L.; Lumpkin, G. R.; Blackford, M. G.; Colella, M.; Zaluzec, N. J. *J. Appl. Phys.* **2008**, *103*, 083531.
(42) Thomas, B. S.; Marks, N. A.; Harrowell, P. *Phys. Rev. B* **2006**, *74*, 214109.

(e.g., values of 0.01 to 0.1 eV are common for compounds with low T_c values). The data obtained via the use of eq 2 are more consistent with typical values for bulk recrystallization of amorphous pyrochlores and related materials. Other investigators have previously used differential thermal analysis (DTA) to determine activation energies of 0.3−1.0 eV for natural pyrochlores,[43] 1.2 eV for $CaPuTi_2O_7$ (^{238}Pu experiment),[44] and 5.8 eV for $Gd_2Ti_2O_7$ doped with ^{244}Cm.[45] The accuracy of the DTA method for determination of the activation energy is an issue here; however, it is also important to consider that thermal annealing of bulk amorphous material and ion irradiation of thin crystals are very different processes. In the latter case, the thin TEM specimen under irradiation is subject to external forcing by irradiation processes (both electronic and nuclear stopping) and the annealing kinetics may be influenced by the higher surface area to volume ratio (e.g., about 4−5 orders of magnitude greater than centimeter sized bulk samples). With this in mind, it may not be surprising to find lower activation energies for the irradiated TEM specimens.

5. Conclusions

The large decrease (nearly 800 K) in measured T_c of the YTS pyrochlore series with increasing Sn content, for ion irradiation with 1.0 MeV Kr ions, appears to be largely due to differences in the combined anion-Frenkel and cation-antisite disorder energy. In support of this inference, the specimen with $x = 1.6$ appears to disorder to the defect fluorite subcell at a low fluence and then remains crystalline up to a fluence of 5×10^{15} ions cm^{-2} upon irradiation at 50 K. Ion irradiation experiments for selected NTZ and LYH samples indicate that the energetics of cation/anion disorder also play a major role in determining the radiation response of these pyrochlore compounds. Chemical bonding, based on the Pauling electronegativity scale, only has a minor effect on radiation tolerance in the YTS and NTZ pyrochlores. At present, we find no compelling evidence to suggest that T_c in the YTS system is nonlinear in composition (the same conclusion applies to the GTZ system). Collectively, the observed T_c values of pyrochlores in all three systems reported in this paper are essentially linear in r_A/r_B and $x(48f)$, giving threshold values of these parameters below or above which the thin crystals remain crystalline during irradiation with 1.0 MeV Kr ions respectively. Furthermore, some of the data fall within previously unexplored regions of the A−B cation radius space for III−IV pyrochlores, suggesting that the data may be useful for future refinement of the empirical models. This effort should include studies of pyrochlore compounds with B = Ru and Mo as well as other ternary pyrochlore compounds.

Acknowledgment. The authors thank the IVEM-Tandem Facility staff at Argonne National Laboratory for assistance during the ion irradiation work. The IVEM-Tandem Facility is supported as a User Facility by the U.S. DOE, Basic Energy Sciences, under Contract W-31-10-ENG-38. We acknowledge financial support from the Access to Major Research Facilities Programme (a component of the International Science Linkages Programme established under the Australian Government's innovation statement, Backing Australia's Ability). Part of this work was supported by the Cambridge-MIT Institute (CMI), British Nuclear Fuels Limited (BNFL), and EPSRC Grant (EP/C510259/1) to G.R.L. We are grateful to Huijun Li and Joel Davis for assistance with the SEM and TEM work and maintenance of the facilities at ANSTO.

(43) Lumpkin, G. R.; Foltyn, E. M.; Ewing, R. C. *J. Nucl. Mater.* **1986**, *139*, 113–120.
(44) Foltyn, E. M.; Clinard, F. W. J.; Rankin, J.; Peterson, D. E. *J. Nucl. Mater.* **1985**, *136*, 97.
(45) Weber, W. J.; Wald, J. W.; Matzke, H. *J. Nucl. Mater.* **1986**, *138*, 196–209.